AIAA JOURNAL
Vol. 46, No. 5, May 2008

Optical Method for Measuring Low Wall Shear Stresses Using Thermal Tufts

J. W. Gregory,* J. W. Baughn,† C. O. Porter,‡ and A. R. Byerley§
U.S. Air Force Academy, Colorado Springs, Colorado 80840

DOI: 10.2514/1.29876

A thermal tuft method for the measurement of low wall shear stresses is described. Previous work described how the thermal tuft method can be used for flow visualization, but this work extends the technique to quantitative measurements of low values of wall shear stress. The laser thermal tuft involves heating a spot on a surface with a laser, which produces a teardrop-shaped surface temperature distribution pointing downstream of the heated spot. The temperature profile can be determined with liquid crystals, infrared thermography, or other methods. In the present study, it is demonstrated by theory and experiment that the lengths of these teardrop-shaped tufts are determined by the wall shear stress. Theoretical results evaluate the effects of laser power, laser spot size, and liquid crystal cutoff temperature on the tuft length. Effects of the thermal boundary-layer thickness are evaluated and found to be negligible for heights up to half of the hydrodynamic boundary-layer thickness. Experimental results agree with theoretical predictions, indicating shorter tuft lengths as shear stress increases. Thermal tufts can be used to measure the wall shear stress at multiple locations, thereby mapping out the wall shear stress distribution.

Nomenclature

c_p	=	specific heat at constant pressure, J/kg · K
d	=	diameter of the laser-heated spot, mm
k	=	thermal conductivity, W/m · K
L	=	tuft length, m
q''	=	convective heat flux, W/m^2
T	=	temperature, °C
T_s	=	surface temperature, °C
T_∞	=	ambient temperature, °C
u	=	x component of velocity, m/s
v	=	y component of velocity, m/s
x	=	coordinate in the streamwise direction, m
y	=	coordinate in the vertical direction, m
z	=	coordinate in the spanwise direction, m
α	=	thermal diffusivity, m^2/s
λ	=	laser wavelength, nm
μ	=	dynamic viscosity, kg/s · m
ρ	=	density of air, kg/m^3
τ	=	wall shear stress, N/m^2
υ	=	kinematic viscosity, m^2/s

I. Introduction

SURFACE flow visualization is useful for understanding flow in many applications and can be used to complement and validate computational studies of complex flow. One nonintrusive surface flow visualization method is the laser thermal tuft. This method was first described by Baughn et al. [1] in a study to determine where flow separation had occurred on the suction side of a turbine blade at low Reynolds numbers (high-altitude operation). The technique was developed because traditional surface flow visualization techniques such as yarn tufts and oil/titanium-dioxide streaks were not successful in identifying separation. Yarn tufts were too large for the very thin separation bubble, often giving a false attached-flow indication because they protruded from the top of the separation bubble. Oil/titanium-dioxide streaks failed to react to the low wall shear stress present during the low-velocity testing (less than 5 m/s). The laser thermal tuft reacted clearly in this low wall shear stress regime. The laser thermal tuft was later patented by the U.S. Air Force (Rivir et al. [2]). This work builds on the previous flow visualization studies by developing the laser thermal tuft technique for shear stress measurements. Both analysis and experiments in a low-speed wind tunnel demonstrate that the length of the thermal tuft depends on shear stress. This concept is then the basis for development of the thermal tuft as a shear stress measurement technique.

A thermal tuft is defined here as a teardrop-shaped temperature pattern on a surface, originating from a heated or cooled spot, pointing in the direction of the surface flow. A typical experimental example of a thermal tuft is shown in Fig. 1 [3]. The thermal tuft is generated by advection causing the heated or cooled air to change the temperature distribution on the surface downstream of the spot. The region surrounding the thermal tuft involves heat transfer by both convection and conduction. Downstream advection of heat is the primary mechanism for tuft generation, as shown in the conceptual diagram in Fig. 2.

The original principle behind the laser thermal tuft was to use a laser to heat a spot on a surface coated with thermochromic liquid crystals. This circular heated laser spot (~3-mm diameter) created a distinct thermal pattern or tuft in the direction of the surface airflow by advection. The thermal tuft is produced by a teardrop-shaped color change in the thermochromic liquid crystals pointing in the downstream direction. Using the laser thermal tuft, Baughn et al. [1] were able to determine the location of boundary-layer separation on a turbine blade model in a cascade wind tunnel. They pointed out that multiple spots could be obtained by using a laser tuft matrix. In the location of boundary-layer separation or reattachment, the thermal tuft is circular and centered around the laser spot, with no hint of a teardrop shape. Further demonstrations of the laser thermal tuft were done by Townsend [4].

Presented as Paper 0647 at the 44th AIAA Aerospace Sciences Meeting and Exhibit, Reno, NV, 9–12 January 2006; received 20 January 2007; revision received 20 December 2007; accepted for publication 3 January 2008.

*Visiting Research Scientist, Department of Aeronautics; currently Assistant Professor, Department of Aerospace Engineering, The Ohio State University, Bolz Hall, 2036 Neil Avenue, Columbus, OH 43210-1276; jim.gregory@alumni.purdue.edu. Member AIAA.

†Distinguished Visiting Professor, Department of Aeronautics, 2354 Fairchild Drive, Suite 6H22; Professor Emeritus, Department of Mechanical and Aeronautical Engineering, University of California, Davis. Associate Fellow AIAA.

‡Graduate Student, Contracted Researcher, Department of Aeronautics, 2410 Faculty Drive, Suite 106. Student Member AIAA.

§Professor, Department Head, Department of Aeronautics, 2354 Fairchild Drive, Suite 6H22. Associate Fellow AIAA.

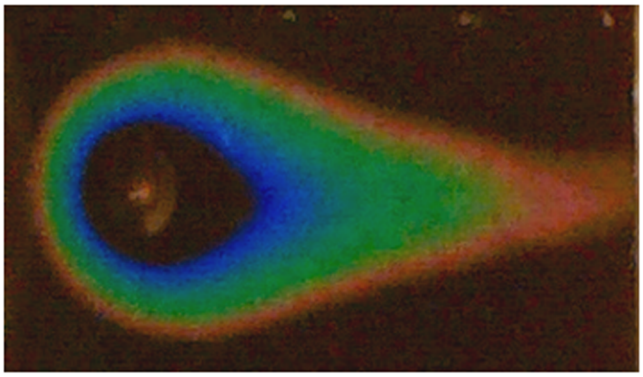

Fig. 1 Laser thermal tuft (Gregory and Peterson [3]).

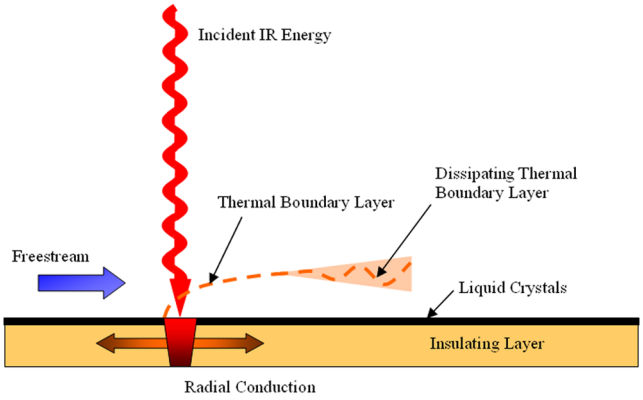

Fig. 2 Diagram of the thermal tuft concept (after Gregory and Peterson [3] and Smith et al. [11]).

Later, Baughn et al. [5] presented results for a laser thermal tuft created by an infrared (IR) laser showing the flow separation and reattachment on a turbine blade at low Reynolds numbers. The IR laser produced a circular spot at the center of the thermal tuft. Their results are shown in Fig. 3. For the Baughn et al. case, in which freestream turbulence was 0.5%, separation occurred at location 2 and reattachment occurred at location 4. Between locations 2 and 4 was a region of recirculation, indicated by the tail of the thermal tuft pointing in the opposite direction of freestream velocity at location 3. At high freestream turbulence (10%), they were able to show that the flow remained attached (the laser tuft images all point in the direction of the freestream flow). These laser thermal tufts were done on vertical surfaces and produced symmetrical thermal tufts. Based on this observation, it was concluded for these cases that buoyancy effects were negligible.

Further applications of the laser thermal tuft were done by Butler et al. [6] and Byerley et al. [7]. These studies also used the laser thermal tuft to determine the location of flow separation and reattachment. In addition, Byerley et al. introduced a dimensionless term to quantify the strength of the laser tuft called "eccentricity." There have been a number of variations on ways to heat or cool the spot and subsequently to observe the resulting thermal tuft. Batchelder and Moffat [8] described the use of heat-sink sources in the form of "pin fins" attached to a heated base to create an array of small hot spots on a surface. They also observed the thermal tufts using liquid crystal thermography. A "cool" thermal tuft was produced by Byerley et al. [9] and IR heaters were used to uniformly heat a black surface with reflective spots affixed to the surface. The reflective spots remained cool, whereas the surrounding surface heated up and produced a thermal tuft downstream of the cool spot. They also used liquid crystal thermography to observe the thermal tuft. Smith et al. [10] used an encapsulated phase change material to produce the cool spot. They used both liquid crystal thermography and infrared thermography to observe the thermal tuft. Smith et al. [11] also produced a cool spot using evaporative cooling. Gregory and Peterson [3] used a laser to produce the heated spot and employed liquid crystal thermography and temperature-sensitive paint to observe the thermal tuft. They also introduced a new variation based on thermal ablation of the substrate material. Their laser thermal tuft using liquid crystal thermography is shown in Figure 1. The tuft shape and size is typically determined by a thin yellow line that occurs between green and red. The length of the tuft shown in Fig. 1 is about 1 cm.

From the earliest experiments with laser thermal tufts (Baughn et al. [1] and Townsend [4]), it was observed that the length of the thermal tuft was affected by the measurement location on a flat plate and the freestream velocity. This was particularly evident in Fig. 11 of [4], in which the tuft length varied along a flat plate with a constant freestream velocity. The cause of this observed variation in length was unknown at the time, although boundary-layer effects were suspected. Hunt and Pantoya [12] suggested that the thermal tuft length can be used as an anemometer to measure the freestream velocity. They measured the tuft length at one axial position as they varied the velocity. Their measurements show the length of the thermal tuft at a fixed axial position on a flat plate increasing with increasing velocity. This trend is in the opposite direction of the measurements presented by Gregory and Peterson [3] and Baughn et al. [13], in which the tuft length decreased when the velocity increased. The reason for the opposite trend reported by Hunt and Pantoya [12] is unknown. In this paper, a theoretical basis is presented for expecting the tuft length at a fixed axial position to decrease when the velocity is increased. It is also demonstrated in this work that the thermal tuft length is determined by the velocity gradient at the surface and the corresponding wall shear stress, not the freestream velocity.

The teardrop pattern of the laser thermal tuft was initially attributed to advection (Baughn et al. [1]), although the details of the advection process and pattern were unknown. To explain the teardrop pattern, Hunt and Pantoya [12] suggested the presence of downstream mixing zones. It is demonstrated in the present paper that conduction and convective transport in a thin layer near the surface (subboundary layer, without mixing) fully account for the teardrop pattern of the laser thermal tuft.

It is also conclusively demonstrated in this paper (both theoretically and experimentally) that the thermal tuft length correlates directly with (and therefore can measure) wall shear stress. This characteristic of the laser thermal tuft was first reported by Baughn et al. [13], whereas the present paper includes new

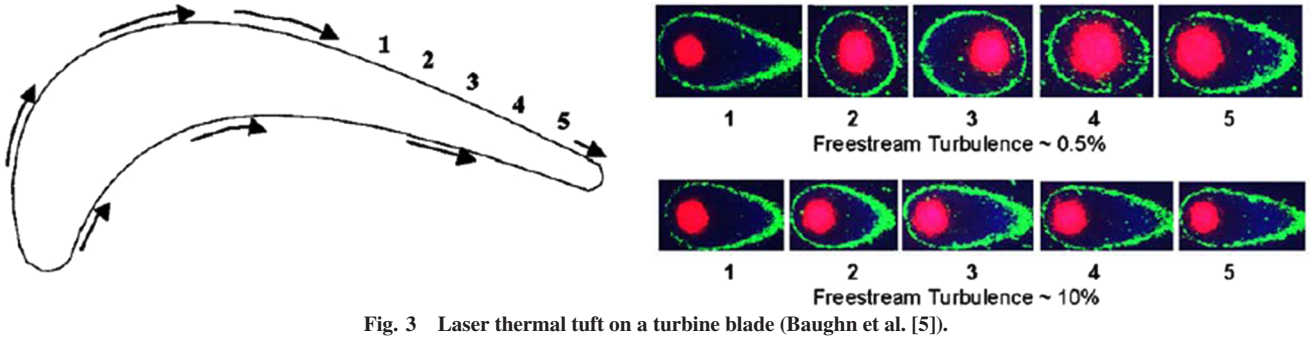

Fig. 3 Laser thermal tuft on a turbine blade (Baughn et al. [5]).

theoretical and experimental results. The shear stress dependency of the laser thermal tuft length greatly enhances its utility as a quantitative measurement technique. Furthermore, it is an optical technique that is particularly useful for measurement of low values of shear stress (less than 1 N/m^2).

Although there are many different ways of measuring wall shear stress, few work well for measurement of such low values. Naughton and Sheplak [14] provided a comprehensive review of shear stress measurement techniques including microelectromechanical system sensors, oil-film interferometry, and liquid crystal sensors. Other key review papers covering shear stress measurement techniques were given by Winter [15] and Haritonidis [16]. In a more recent conference paper, Plesniak and Peterson [17] provided an integrative compilation of wall shear stress measurement techniques and their limitations. At the same conference, Hakkinen [18] reflected on early skin-friction measurements. It should be noted that the definition of thermal tufts in this paper is different than that of Eaton et al. [19], who described two instruments for flow direction and skin-friction measurements in separated flows. They cleverly used a pulsed wall probe to measure time-dependent skin friction and a thermal tuft to determine instantaneous flow direction. Their pulsed wall probes and thermal tuft used three fine wires (a heater and two sensors) mounted slightly above a surface to detect skin friction and flow direction. The advantage of the thermal tufts described in the present paper is that they do not require any wires because they use optical methods and are hence relatively nonintrusive. The advantage of the instruments by Eaton et al. [19] is that they measured time-dependent values with a relatively high frequency response, whereas the thermal tufts described here measure only the time-averaged values. One optical technique that also uses a laser to heat a spot is described by Oosthuizen and Carscallen [20]. They correlate wall shear stress with the cooling rate of their heated spot. Mayer [21] also employed a laser-heated spot for shear stress measurements, but recorded the wall temperature of the heated spot using IR thermography to infer shear stress.

Optical methods such as the laser thermal tuft have several advantages, including the ability to make measurements at many discrete locations to establish wall shear stress distributions, the ability to select and change those locations during testing, and (for the most part) a lack of intrusiveness. The results in this paper demonstrate that the thermal tuft length is correlated directly with wall shear stress.

II. Theory

The purpose of the present research is to demonstrate conclusively that thermal tuft length correlates directly with wall shear stress. The theoretical basis for expecting that thermal tuft size is dependent on the velocity gradient at the surface, and therefore the wall shear stress, is described. Measurements of the tuft length are correlated with wall shear stresses in the next section.

To demonstrate that the laser thermal tuft length for a given fluid (air in this case) is a function only of the surface velocity gradient du/dy, and therefore only the wall shear stress, a two-dimensional solution for the temperature distribution in the air and along the surface downstream of a heated zone is determined in the manner described next.

The energy equation for a boundary layer, neglecting transport in the z direction, is given by [22]

$$u\frac{\partial T}{\partial x}+v\frac{\partial T}{\partial y}=\alpha\frac{\partial^2 T}{\partial y^2}+\frac{\upsilon}{c_p}\left(\frac{\partial u}{\partial y}\right)^2 \tag{1}$$

Neglecting the viscous dissipation term (the second term on the right-hand side) and assuming that $u(\partial T/\partial x) \gg v(\partial T/\partial y)$, the equation becomes

$$u\frac{\partial T}{\partial x}=\alpha\frac{\partial^2 T}{\partial y^2} \tag{2}$$

The validity of the assumption that the first term is much larger than the second term of Eq. (1) was evaluated and found to be the case for the laminar boundary layer and temperature gradients involved in these simulations.

Because the hydrodynamic boundary-layer thickness changes very little over the distance of the laser thermal tuft, it can be assumed that u is not a function of x; that is, $u = u(y)$ only. Assuming that the thermal effects are limited to a thin region of the boundary layer near the surface (on the order of 10–20% of the thickness of a laminar boundary layer or the thickness of the viscous sublayer for a turbulent boundary layer) and that a no-slip condition exists at the surface, the velocity $u(y)$ is given by

$$u=\frac{du}{dy}y \tag{3}$$

The validity of this assumption will be evaluated later. Substituting into Eq. (2), the energy equation becomes

$$\left(\frac{du}{dy}\right)y\frac{\partial T}{\partial x}=\alpha\frac{\partial^2 T}{\partial y^2} \tag{4}$$

This can be solved for the temperature distribution in the air, $T(x, y)$, using an explicit method. The boundary conditions used here are for a circular spot with a uniform heat flux (corresponding to laser heating of a spot on an insulated surface), with the rest of the surface insulated, as illustrated in Fig. 4.

For a circular heated spot,

$$-k\,dT/dy=q'' \tag{5a}$$

and elsewhere on the surface,

$$-k\,dT/dy=0 \tag{5b}$$

From the solution, the constant du/dy assumption can be checked by determining the y distance over which a significant temperature gradient exists, which will be evaluated in a following section. Because the wall shear stress is given by

$$\tau=\mu\frac{du}{dy} \tag{6}$$

each selection of a du/dy corresponds to a particular wall shear stress.

Solutions for the surface temperature distribution for $du/dy = 2000\ s^{-1}$ and $du/dy = 4000\ s^{-1}$ (which, for air, corresponds to wall shear stresses of 0.072 and 0.143 N/m^2, respectively) are shown in Fig. 5 using an ambient temperature of 20°C and constant properties for air. In air, these velocity gradients would occur for a laminar boundary layer with velocities of 5 and 8 m/s at a distance of 22 cm from the leading edge of a flat plate. These simulation results were compiled from a series of 200 spanwise heated strips, with the chordwise length of each strip corresponding to a cross section of the heated circular spot. The higher the value of wall shear stress, the shorter the length of the tuft.

A comparison of Fig. 5 with Fig. 1 shows the great similarity between the theoretical solutions (Fig. 5) and the experimental images of a laser thermal tuft image (Fig. 1). There are several minor

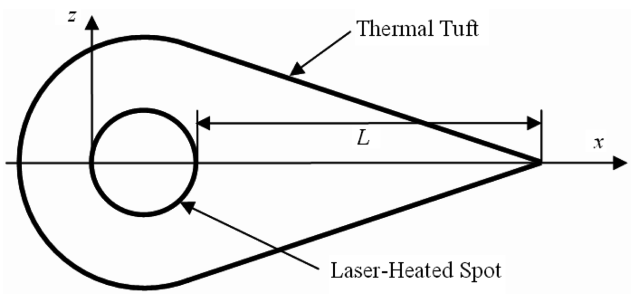

Fig. 4 Diagram showing the laser thermal tuft configuration.

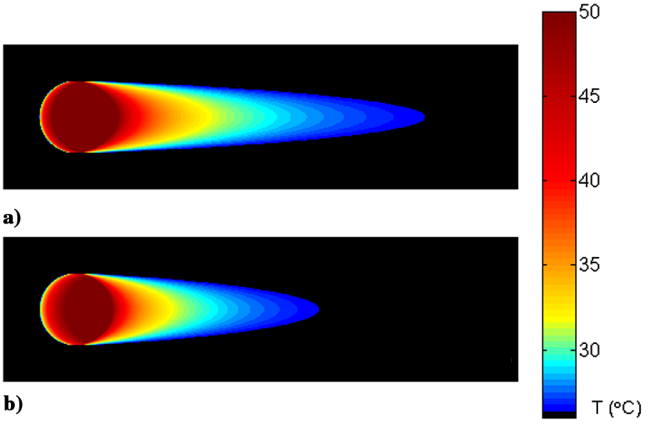

Fig. 5 Theoretical solution showing dependence of tuft length on wall shear stress; $T_\infty = 20°C$, $q'' = 3500\ W/m^2$, and $d = 3$ mm: a) $\tau = 0.072\ N/m^2$ and b) $\tau = 0.143\ N/m^2$.

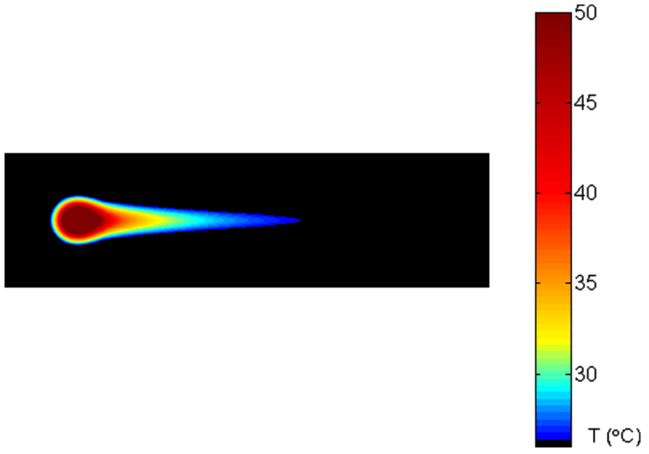

Fig. 6 Effect of Gaussian heating distribution on the thermal tuft profile; $T_\infty = 20°C, q'' = 3500\ W/m^2, d = 3$ mm, and $\tau = 0.143\ N/m^2$.

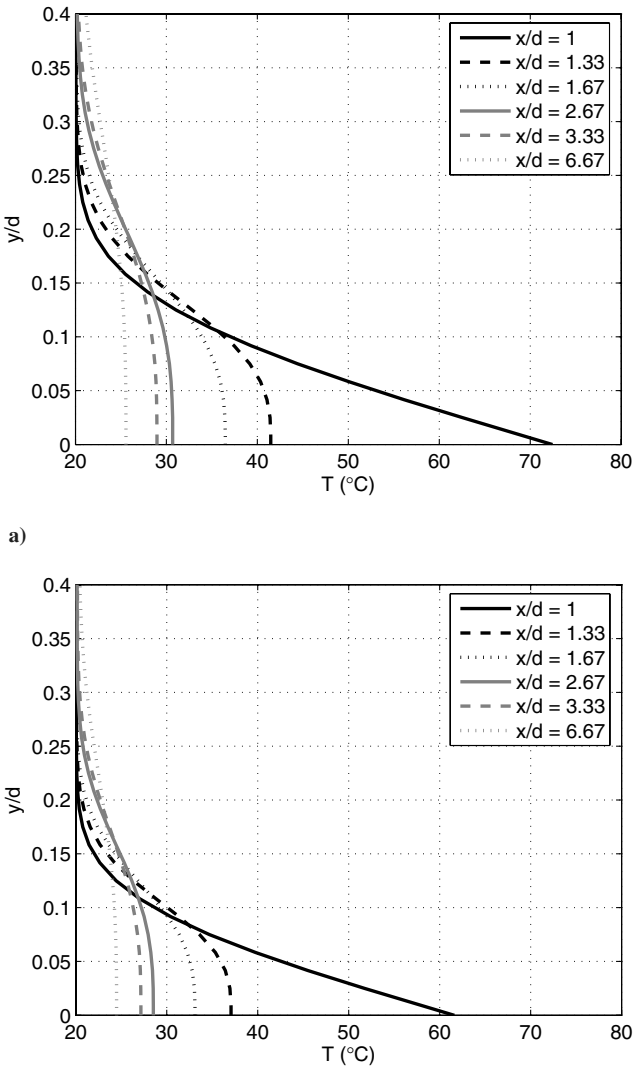

Fig. 7 Temperature profiles in the thermal boundary layer, $T_\infty = 20°C$, $q'' = 3500\ W/m^2$, $d = 3$ mm: a) $du/dy = 2000\ s^{-1}$ ($\tau = 0.072\ N/m^2$) and b) $du/dy = 4000\ s^{-1}$ ($\tau = 0.143\ N/m^2$); the downstream edge of the heated spot is at $x/d = 1$.

differences. One is the presence of wall conduction in the image of Fig. 1, which is not accounted for in the theoretical treatment. This causes color change slightly upstream of the heated spot and may skew the tuft length slightly. It should also be noted that a uniform heat flux for the heated spot was assumed for the theoretical treatment, whereas the laser has more of a Gaussian heating distribution on the spot. The effect of a Gaussian heating distribution is shown in Fig. 6. The edges of the heated spot contribute much less heating to the flow; thus, the theoretical profile of the tuft becomes thinner, with an apparent "pinched" effect downstream. Experimental instances of thermal tufts, however, exhibit a profile much closer to those seen in Fig. 5. This may be attributed to heat conduction within the substrate dominating any effects from a Gaussian heating distribution. Therefore, all further analysis will assume a uniform heating distribution within the area of the laser-heated spot.

To understand the effect of du/dy (and therefore wall shear stress) on the tuft length seen in Fig. 5, the solutions for the temperature distribution in the air along the centerline of the tuft ($z = 0$) are shown in Fig. 7. The temperature distribution at 3 mm ($x/d = 1$) shows the high surface temperature at the end of the heating length of 3 mm. The subsequent temperature distributions are for an insulated surface (thus the zero temperature gradient at the surface). Near the surface, the temperature decreases with increasing distance downstream. This is also reflected in the surface temperature distributions shown in Fig. 5. In the upper portion of the thermal boundary layer (see Fig. 7) the temperature increases slightly with downstream distance. This is a consequence of the conductive and convective heat transport in the thermal boundary layer downstream of the heated region. Comparing Figs. 7a and 7b, it is seen that as the wall shear stress (and the velocity gradient) increases, the surface temperature decreases more rapidly downstream, resulting in a decrease in the tuft length. This is a consequence of the increased convective transport in the boundary layer as du/dy is increased.

Note that the thickness of the thermal boundary layer is quite small compared with a typical hydrodynamic boundary-layer thickness, which is an important criterion for the linear velocity gradient assumption employed in the derivation of Eq. (4). The error induced by a nonlinear velocity gradient is quantitatively evaluated in Fig. 8. Here, varying portions of a laminar boundary layer were included in the analysis to evaluate the impact on the predicted tuft length. As long as the thermal boundary layer is less than half the thickness of the hydrodynamic boundary layer, then the error in tuft length is less than 1% (for a wide range of shear stresses). This also validates the assumption that transport in the z direction is negligible.

The surface temperatures for the centerline $z = 0$ are plotted as a function of downstream distance x in Fig. 9 for the two values of wall shear stress. The region from 0 to 3 mm ($x/d = 1$) is located within the heated spot, in which the constant-heat-flux boundary condition is employed. The surface temperature in this region continues to increase until the end of the heated spot. From $x = 3$ mm ($x/d = 1$) and moving downstream, the surface temperature rapidly decreases. The properties of the thermochromic liquid crystals determine the tuft length for a given surface temperature profile (i.e., wall shear stress). Thus, if the liquid crystal cutoff temperature were selected as

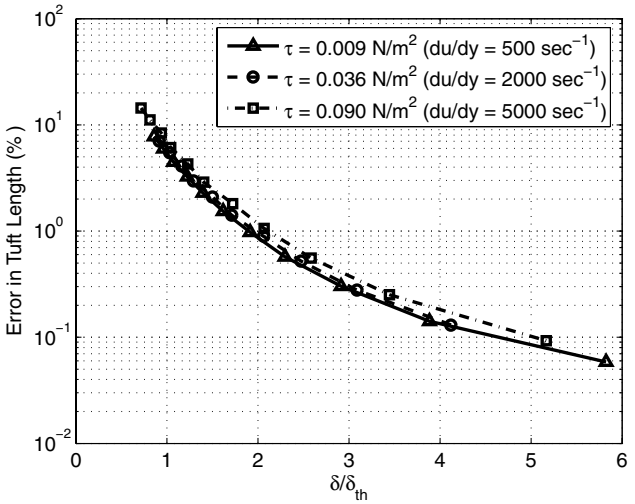

Fig. 8 Error in tuft length due to varying thickness of the thermal boundary layer; $T_\infty = 20°C$, $q'' = 3500$ W/m^2, and $d = 3$ mm.

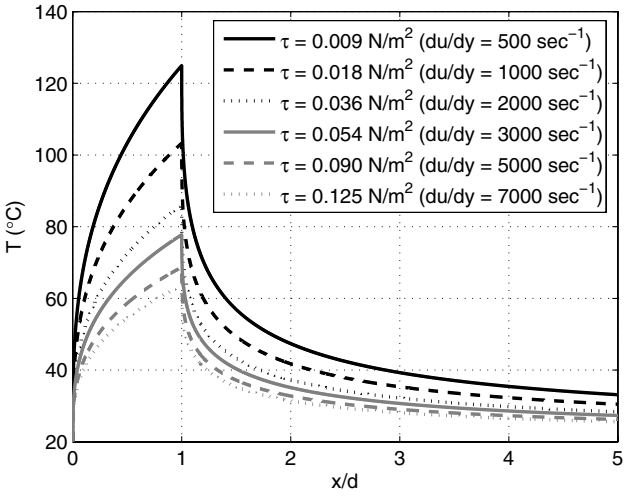

Fig. 10 Effect of wall shear stress on the surface temperature along the centerline ($z = 0$); $T_\infty = 20°C$, $q'' = 3500$ W/m^2, and $d = 3$ mm; the downstream edge of the heated spot is at $x/d = 1$.

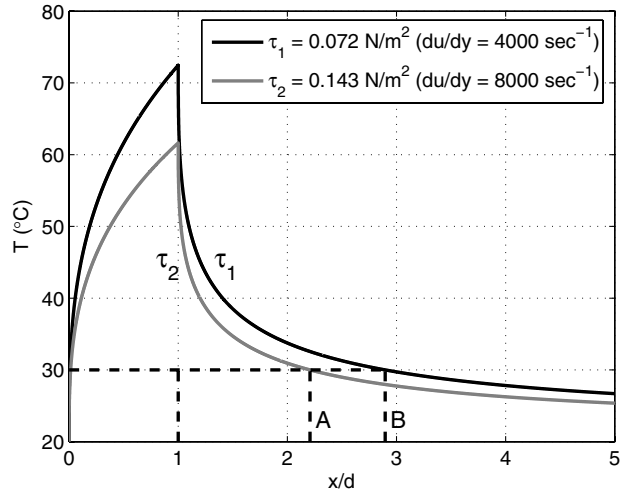

Fig. 9 Theoretical variation of tuft length with wall shear stress along the centerline ($z = 0$; $T_\infty = 20°C$, $q'' = 3500$ W/m^2, and $d = 3$ mm; the downstream edge of the heated spot is at $x/d = 1$.

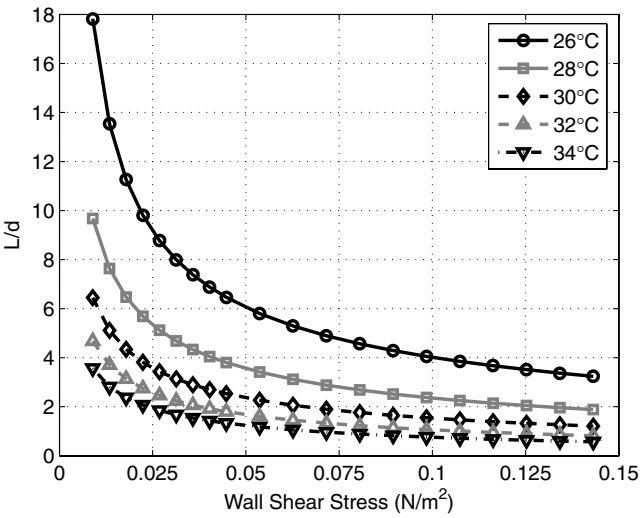

Fig. 11 Effect of liquid crystal cutoff temperature on sensitivity of tuft length to wall shear stress; $T_\infty = 20°C$, $q'' = 3500$ W/m^2, and $d = 3$ mm.

30°C (with an ambient temperature of 20°C), the lengths of the tuft for each du/dy (or wall shear stress) are points A and B in Fig. 9. As seen in Fig. 9 for the higher-wall shear stress case τ_2, the length of the heated region is shorter than that of the lower-wall shear stress case τ_1. This means that as wall shear stress increases, the tuft length decreases, assuming that the heat flux is held constant. This also means that at a fixed axial position, if the velocity is increased, the tuft length will decrease as the wall shear stress increases. Figure 10 shows a series of curves that represent the surface temperature distribution for varying wall shear stress. Note that the most significant variation in tuft length occurs at low values of the wall shear stress.

To illustrate the sensitivity of the laser thermal tuft method for measuring wall shear stress, the tuft length is plotted as a function of wall shear stress in Fig. 11. Several cutoff temperatures were selected, representing various hypothetical formulations of thermochromic liquid crystals. The tuft length becomes significantly longer and the sensitivity of the technique increases as the cutoff temperature approaches the ambient temperature. These findings suggest that the highest-quality experimental results (longest tuft length and highest sensitivity to wall shear stress) may be obtained when the cutoff temperature is slightly above ambient conditions. This requires careful control of the ambient conditions. Thus, the selection of the liquid crystal cutoff temperature relative to ambient temperature is driven by the tradeoff between sensitivity and uncertainty. This behavior also highlights the importance of careful measurement and control of the ambient temperature. Any drift in ambient temperature can induce errors in the indicated wall shear stress.

The physical reason for higher sensitivity when the cutoff temperature is closer to ambient temperature is elucidated by Fig. 9. The natural temperature profile generated downstream of the laser-heated spot rapidly decays in an exponential-like fashion, with a long tail. In this region of very low dT/dx, the tuft length will be very sensitive to a change in shear stress. This is demonstrated by examining the difference in tuft length if the cutoff temperature is 40°C versus the cutoff of 30°C, illustrated in Fig. 9. The change in tuft length is much less for the higher liquid crystal cutoff temperature for the same set of wall shear stress conditions.

Note that the sensitivity of the technique is much greater for low values of wall shear stress. At some point, however, the sensitivity will decrease back to zero when the wall shear stress decreases to zero. The slope of the velocity gradient becomes very low as shear stress approaches zero, and little heat is advected downstream. In this limiting case, the laser-heated spot will become axisymmetric because conduction through the substrate will dominate any downstream advection. Thus, there is an experimental limit, depending on conduction effects, at which the sensitivity stops

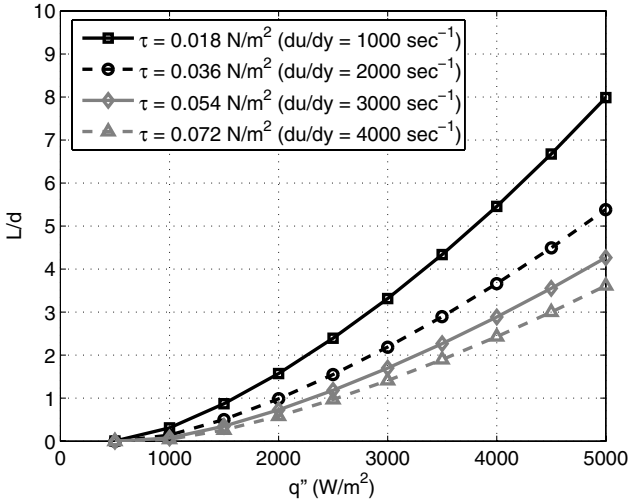

Fig. 12 Effect of convective heat flux (determined by laser power) on tuft length; $T_\infty = 20°C$ and $d = 3$ mm.

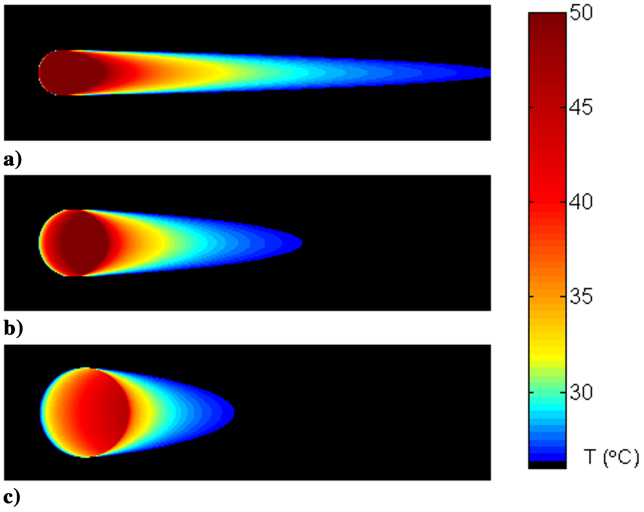

Fig. 13 Effects of the laser-heated spot diameter on the thermal tuft profile, with incident laser power held constant for spot diameters of a) 2 mm ($q'' = 7875$ W/m^2), b) 3 mm ($q'' = 3500$ W/m^2), and c) 4 mm ($q'' = 1970$ W/m^2); $T_\infty = 20°C$.

increasing and instead decreases to zero as wall shear stress values approach zero.

The effect of the heat flux (laser power) on tuft length is shown in Fig. 12. For this example, an ambient temperature of 20°C and a liquid crystal cutoff temperature of 30°C are assumed. As would be expected, higher heat fluxes (laser power) result in higher surface temperatures and correspondingly longer tufts. This effect was experimentally observed and reported by Hunt and Pantoya [12]. They calculated that 7 mW was required for their thermal tuft (assuming a fully developed thermal boundary layer, which, as already shown, does not occur) and reported using 50 and 90 mW with a 6-mm laser spot size, corresponding to 1800 and 3200 W/m^2, respectively. The earlier measurements by Baughn et al. [5] used approximately 80 mW for the laser power with a spot size of 3 mm, corresponding to a heat flux of 11,300 W/m^2. The theoretical tuft shown in Fig. 5 assumed a convective heat flux of 3500 W/m^2, which corresponds to 25 mW for a 3-mm-diam heated spot. The required power will be higher than this due to reflection, radiation, and conduction losses. The absorptivity of the liquid-crystal-coated surfaces is generally high. The radiation and conduction losses depend on the temperatures chosen for the liquid crystal and on the insulation properties of the wall. The laser power requirement is also dependent on the spot size and the velocity gradient (wall shear stress).

The diameter of the laser-heated spot is an important parameter governing the tuft length, as shown in Fig. 13. Here, the incident laser power was held constant, but the size of the laser spot was varied. Thus, the heat flux increases as the spot diameter decreases. This analysis is analogous to focusing a laser beam of fixed power to a smaller spot size. The results in Fig. 13 demonstrate that the tuft is much longer for a smaller laser spot size. As the spot size decreases, the streamwise heated length decreases proportionally with spot diameter d. This would be expected to decrease the tuft length (opposite to that observed). However, because laser power is held constant as the heated area decreases (smaller spot), there is also a higher heat flux. In fact, the heat flux increases proportionally with the diameter squared d^2. Of these two competing trends, the increased heat flux dominates and the tuft length increases with a smaller laser-heated spot.

III. Experiment

An experimental test of the shear stress dependency was performed to validate the theory and help resolve the discrepancy between the results of Gregory and Peterson [3] and Hunt and Pantoya [12]. Gregory and Peterson [3] reported that tuft length decreases with velocity, whereas Hunt and Pantoya [12] reported results of the opposite trend. Both sets of results, however, correlated tuft length with velocity, whereas the current work demonstrates

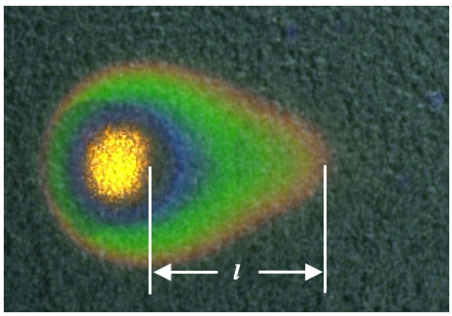

Fig. 14 Indication of the thermal tuft length.

conclusively that this is erroneous because the correlation of tuft length is with shear stress. This experimental work also demonstrates the implementation of the thermal tuft for quantitative measurements and provides an indication of the sensitivity of the technique.

The experimental verification of the tuft-length shear stress dependency demonstrated theoretically was performed on a flat plate coated with liquid crystals exposed to a freestream of varying velocity. The flat plate consisted of an insulating foam board placed on the bottom wall of a 30×30 cm wind-tunnel test section, extending upstream into the contraction and smoothly faired with the contraction wall. The foam board was painted with a flat black base coat, which was subsequently airbrushed with Hallcrest R24C10W thermochromic liquid crystals. A 65-mW IR laser ($\lambda = 1064$ nm) induced an area of constant heat flux on the surface of the flat plate. A set of cool white fluorescent bulbs illuminated the surface of the liquid crystals. Thermal tufts formed on the surface of the flat plate were recorded with a Nikon D1 digital camera with a 105-mm lens, after the laser had illuminated the surface for a period sufficient for a steady-state thermal tuft to be reached (on the order of 30 s). The physical tuft length was evaluated by calibrating the pixel size with an imaged scale and by determining the distance between the edge of the laser-heated spot and the end of the red color band, as illustrated in Fig. 14. Both positions were precisely determined by examining a cross-sectional plot of the red channel of the color image, and selecting the points at which the intensity value was 100 counts (out of the 8-bit resolution of the image).

The wind-tunnel test section velocity was set to varying levels to control the wall shear stress. Test section velocities of 4.4, 5.9, 7.7, 9.2, 11.3, 13.2, and 15.4 m/s (for a Reynolds number range of 100,000 to 340,000, based on a distance of 0.42 m downstream from the leading edge of the flat plate) were selected to span the capability

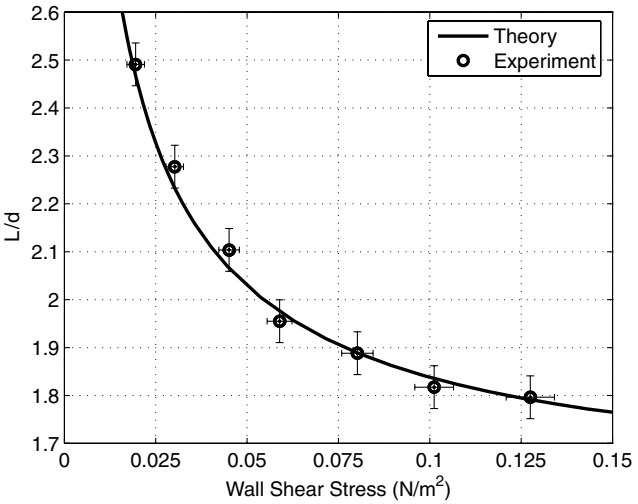

Fig. 15 Measured effect of wall shear stress on the thermal tuft length, compared with a theoretical solution for the same conditions: $T_\infty = 19°\text{C}$, $q'' = 3500\ \text{W/m}^2$, and $d = 3\ \text{mm}$.

range of the wind tunnel. The wall shear stress was determined for each test velocity by measuring the boundary-layer profile with a traversed narrow-gage pitot probe. Blasius profiles were fit to each of the measured boundary-layer profiles to conclusively confirm that laminar flow was present for all test conditions. This was found to be the case throughout the entire velocity range. These Blasius profiles were then used to determine the velocity gradient at the wall. The resulting shear stress spanned a range from 0.02 to 0.13 N/m^2, and the resulting boundary-layer thickness ranged from approximately 3 to 6 mm. The corresponding thermal boundary-layer thickness, as estimated by the solution of the energy equation, ranged from 0.26 to 1.1 mm. For these experiments, the ratio of the hydrodynamic and thermal boundary-layer thicknesses was at least 5.6.

Results from this set of experiments are shown in Fig. 15. Tuft lengths at one fixed location were measured as the velocity was varied, and the tuft length was found to decrease in response to increasing shear stress (and velocity). As theoretically predicted, the measured response to velocity is opposite to that reported by Hunt and Pantoya [12] (i.e., the tuft length decreased when the velocity was increased), but agrees with the findings of Gregory and Peterson [3]. The tuft length was longest at the lowest value of wall shear stress (the lowest velocity) and decreased with increasing wall shear stress (higher velocity for a fixed location). The experimental trend that defines the relationship between thermal tuft length and wall shear stress (tuft length decreases with increasing wall shear stress) is again the same as the theoretical results presented in Fig. 11.

Theoretical results are compared with the experiment results in Fig. 15, showing excellent agreement with the experimental relationship between tuft length and wall shear stress. The theoretical solution is based on the following parameter selections, which were all directly measured for the experiments (except as noted). The size of the laser-heated spot was 3 mm in diameter, and laser power was held constant at 65 mW. A loss factor of 90% was assumed for the laser power, which accounts for transmission losses through the Plexiglas wind-tunnel wall, as well as conduction and radiation losses from the heated spot. Ambient temperature and pressure were 19°C and 78.46 kPa, respectively (at an elevation of 2.2 km). Standard properties of air were assumed for dynamic viscosity ($1.7894 \times 10^{-5}\ \text{kg/m} \cdot \text{s}$), thermal conductivity ($0.0263\ \text{W/m} \cdot \text{K}$), and specific heat ($1007\ \text{J/kg} \cdot \text{K}$). A cutoff temperature of 25.7°C was assumed, which is somewhat higher than the cutoff temperature of 24°C specified by the manufacturer for the particular liquid crystals used in the experiments. This higher cutoff temperature was selected because the edge of the tuft was determined by a color in the middle of the red bandwidth of the liquid crystals. An offset of 2 mm was added to the theoretical determination of tuft length as an arbitrary offset. Assumed parameters for laser power loss factor, liquid crystal cutoff temperature, and tuft-length offset were adjusted to optimize the quality of fit. Both the theoretical and experimental results demonstrate a decrease in tuft length with increasing shear stress. The trend is a nonlinear relationship with higher sensitivity at lower values of shear stress.

IV. Implementation and Limitations

The laser thermal tuft technique provides high sensitivity at low values of shear stress, a direct indication of the direction of the shear stress vector, the ability to make measurements at many discrete locations to establish wall shear stress distributions, the ability to select and change those locations during testing, low cost, and low intrusiveness. However, the thermal tuft technique also has several limitations. These constraints must be accounted for when applying the laser thermal tuft to arbitrary test conditions. The current utility of the technique has only been evaluated with steady laminar flows. Application to turbulent flows may be possible, but it requires further investigation. When the thermal tuft method is implemented as a wall shear stress measurement technique, a direct calibration must be preformed against an accepted standard such as a velocity profile measurement. The thermal conductivity of the substrate should be low to minimize radial conduction losses, and the material properties must remain constant across the measurement region. Incident laser power must be held constant at an optimized level that produces the longest tufts possible without burning the liquid crystals, inducing buoyancy effects, or creating a thermal boundary layer greater than half the hydrodynamic boundary-layer thickness. As discussed earlier, the sensitivity of the thermal tuft length can vary depending on the difference between ambient temperature and the cutoff temperature of the liquid crystals. Thus, ambient temperature must be held constant, otherwise temperature drift must be measured and the effects quantified. The technique is generally applicable only to steady flows, due to the slow response associated with the relevant heat transfer mechanisms. The sensitivity of the thermal tuft technique varied in these experiments from 59.9 $\text{mm/(N/m}^2)$ at the lowest value of wall shear stress (0.0195 N/m^2) to 2.4 $\text{mm/(N/m}^2)$ at the highest measured value of wall shear stress (0.1275 N/m^2). Under well-controlled experimental conditions, the measurement in tuft length can be reasonably estimated to be discernible within 0.1 mm, giving an uncertainty in wall shear stress ranging from 0.002 to 0.042 N/m^2 for the preceding conditions. As demonstrated through the theoretical work, the sensitivity may be enhanced by bringing the ambient temperature closer to the liquid crystal cutoff temperature.

V. Conclusions

This work demonstrates that the length of a laser-induced thermal tuft is a direct indication of wall shear stress. Both theoretical and experimental results demonstrated that tuft length decreases with an increase in shear stress. The energy equation was solved for a heated spot with uniform heat flux and a constant velocity gradient $\text{d}u/\text{d}y$ above the wall. The surface temperature distribution determined from the solution of the energy equation matches the thermal tuft distribution observed in experiments. The solutions show that for typical conditions with air that the thermal region affected is on the order of 1.0 mm from the surface, validating the assumption of a constant velocity gradient for most flow conditions. A detailed assessment of the linear velocity gradient assumption reveals that the error in tuft length is less than 1% as long as the thickness of the hydrodynamic laminar boundary layer is at least twice the thermal boundary-layer thickness. Because the hydrodynamic boundary-layer thickness for these experiments was at least 3 mm and the thermal boundary-layer thickness was estimated to be no greater than 1.1 mm, errors due to nonlinearity in the velocity profile are negligible.

The thermal tuft-length correlation with wall shear stress is dependent on the choice of liquid crystal cutoff temperature relative to the air temperature, the laser power, and the spot size. The sensitivity of the thermal tuft for wall shear stress measurements

(change in tuft length per unit change in wall shear stress) is greatest when the liquid crystal cutoff temperature is closest to the air temperature. However, changes in the ambient air temperature will affect the tuft length, requiring careful control of the ambient temperature. Thus, there is a tradeoff between sensitivity and uncertainty caused by changes in the ambient air temperature. The greatest sensitivity (change in tuft length per unit change in wall shear stress) occurs at low values of wall shear stress and was experimentally found to be 59.9 $\mathrm{mm}/(\mathrm{N}/\mathrm{m}^2)$ at a wall shear stress of 0.0195 N/m^2. These results demonstrate that the laser thermal tuft offers a new nonintrusive optical method for measuring low wall shear stresses, in which the length of the thermal tuft is directly dependent on the velocity gradient at the wall and is thus dependent on wall shear stress.

Acknowledgments

J. W. Baughn gratefully acknowledges the support of the Distinguished Visiting Professor program at the U.S. Air Force (USAF) Academy and the help of John Sherfesee, Director of this program. J. W. Gregory gratefully acknowledges the support of a National Research Council Research Associateship Award funded by the U.S. Air Force Research Lab at the USAF Academy. The authors thank John Sullivan and Sean Peterson of Purdue University for helpful discussions on the thermal tuft and recognize John Sullivan's independent conception of the thermal tuft concept. The authors also gratefully acknowledge the efforts of the USAF Academy Cadets Ashmore, Czarniecki, Gertiser, Lay, Miller, and Skinner who assisted with acquiring the experimental data presented in this paper.

References

[1] Baughn, J. W., Butler, R. J., Byerley, A. R., and River, R. B., "An Experimental Investigation of Heat Transfer, Transition and Separation on Turbine Blades at Low Reynolds Number and High Turbulence Intensity," American Society of Mechanical Engineers, Paper 95-WA/HT-25, Nov. 1995.

[2] Rivir, R. B., Baughn, J. W., Butler, R. J., and Byerley, A. R., and Townsend, J. L., "Thermal Tuft Fluid Flow Investigation Apparatus with a Color Alterable Thermally Responsive Liquid Crystal Layer," U.S. Patent No. 5963292, issued Oct. 1999.

[3] Gregory, J. W., and Peterson, S. D., "Flow Visualization with Laser-Induced Thermal Tufts," AIAA Paper 2005-0699, Jan. 2005.

[4] Townsend, J. L., "A Laser Thermal Tuft Using Liquid Crystals for Flow Visualization," M.S. Thesis, Univ. of California, Davis, Davis, CA, 1996.

[5] Baughn, J. W., Mayhew, J. E., Butler, R. J., Byerley, A. R., and Rivir, R. B., "Turbine Blade Flow Separation and Reattachment at Low Reynolds Numbers," *Journal of Heat Transfer*, Vol. 121, Aug. 1999.

[6] Butler, R. J., Byerley, A. R., Van Treuren, K., and Baughn, J. W., "The Effect of Turbulence Intensity and Length Scale on Low-Pressure Turbine Blade Aerodynamics," *International Journal of Heat and Fluid Flow*, Vol. 22, No. 2, 2001, pp. 123–133. doi:10.1016/S0142-727X(00)00081-3

[7] Byerley, A. R., Störmer, O., Baughn, J. W., Simon, T. W., Van Treuren, K. W., and List, J., "Using Gurney Flaps to Control Laminar Separation on Linear Cascade Blades," *Journal of Turbomachinery*, Vol. 125, No. 1, 2003, pp. 114–120. doi:10.1115/1.1518701

[8] Batchelder, K. A., and Moffat, R. J., "Surface Flow Visualization Using the Thermal Wakes of Small Heated Spots," *Experiments in Fluids*, Vol. 25, No. 2, 1998, pp. 104–107. doi:10.1007/s003480050213

[9] Byerley, A. R., Störmer, O., Baughn, J. W., Simon, T. W., and Van Treuren, K. W., "A 'Cool' Thermal Tuft for Detecting Surface Flow Direction," *Journal of Heat Transfer*, Vol. 124, No. 4, 2002, p. 594. doi:10.1115/1.1502631

[10] Smith, J., Baughn, J. W., and Byerley, A. R., "Surface Flow Visualization Using Thermal Tufts Produced by an Encapsulated Phase Change Material," *International Journal of Heat and Fluid Flow*, Vol. 26, No. 3, 2005, pp. 411–415. doi:10.1016/j.ijheatfluidflow.2004.10.004

[11] Smith, J., Baughn, J. W., and Byerley, A. R., "Surface Flow Visualization Using Thermal Tufts Produced by Evaporatively Cooled Spots," *Journal of Fluids Engineering*, Vol. 127, No. 1, 2005, pp. 186–188. doi:10.1115/1.1852493

[12] Hunt, E. M., and Pantoya, M. L., "A Laser Induced Diagnostic Technique for Velocity Measurements Using Liquid Crystal Thermography," *International Journal of Heat and Mass Transfer*, Vol. 47, Nos. 19–20, 2004, pp. 4285–4292. doi:10.1016/j.ijheatmasstransfer.2004.04.026

[13] Baughn, J. W., Byerley, A. R., and Gregory, J. W., "An Optical Method for Measuring Low Wall Shear Stresses Using Thermal Tufts," AIAA Paper 2006-0647, Jan. 2006.

[14] Naughton, J. W., and Sheplak, M., "Modern Developments in Shear-Stress Measurement," *Progress in Aerospace Sciences*, Vol. 38, Nos. 6–7, 2002, pp. 515–570. doi:10.1016/S0376-0421(02)00031-3

[15] Winter, K. G., "An Outline of the Techniques Available for the Measurement of Skin Friction in Turbulent Boundary Layers," *Progress in Aerospace Sciences*, Vol. 18, No. 1, 1977, pp. 1–57.

[16] Haritonidis, J. H., "The Measurement of Wall Shear Stress," *Advances in Fluid Mechanics Measurements*, edited by M. Gad-el-Hak, Springer–Verlag, Berlin, 1989, pp. 229–261.

[17] Plesniak, M. W., and Peterson, S. D., "Wall Shear Stress Measurements for Conventional Applications and Biomedical Flows," AIAA Paper 2004-2301, June 2004.

[18] Hakkinen, R. J., "Reflections on Fifty Years of Skin Friction Measurement," AIAA Paper 2004-2111, Jun. 2004.

[19] Eaton, J. K., Westphal, R. V., and Johnston, J. P., "Two New Instruments for Flow Direction and Skin-Friction Measurements in Separated Flows," *ISA Transactions*, Vol. 21, No. 1, 1982, pp. 69–78.

[20] Oosthuizen, P. H., and Carscallen, W. E., "A Numerical Investigation of a Method of Using Measurements of the Heat Transfer from a Laser Heated Spot to Determine Wall Shear Stress," *Experimental Heat Transfer, Fluid Mechanics, and Thermodynamics 1991*, edited by J. F. Keffer, R. K. Shah, and E. N. Ganic, Elsevier, New York, 1991, pp. 345–352.

[21] Mayer, R., "Orientation on Quantitative IR-Thermography in Wall-Shear Stress Measurements," Faculty of Aerospace Engineering, Delft Univ. of Technology, Rept. LR-812, Delft, The Netherlands, Oct. 1996.

[22] Incropera, F. P., and DeWitt, D. P., *Introduction to Heat Transfer*, 4th ed., Wiley, New York, 1996, p. 310.

R. Lucht
Associate Editor